

Mechanosensitivity of Crawling Cells under Periodically Stretching Substrates

John J. Molina^{1,*} and Ryoichi Yamamoto^{1,2}

¹*Department of Chemical Engineering, Kyoto University, Kyoto 615-8510*

²*Institute of Industrial Science, The University of Tokyo, Tokyo 153-8505*

(Dated: December 14, 2024)

The mechanosensitivity of cells, which determines how they are able to respond to mechanical signals received from their environment, is crucial for the functioning of all biological systems. However, a detailed understanding of such response is still lacking, as it involves processes occurring over a wide range of length- and time-scales. Experimentally, one of the preferred methods to investigate how crawling cells react to such stimulation is to apply cyclic stretching to the substrate to which they are attached. Studying the shape deformations and changes in motility, as well as the localization of characteristic proteins (e.g., actin or myosin) or the orientation of the actin filament network inside of the cell under stretching, has provided crucial information on their mechanosensing abilities. In particular, cells have been shown to reorient under such perturbations, aligning at specific angles with respect to the stretching direction that depends strongly on the type of cell. We introduce a computation model for crawling cells on such periodically stretching substrates that is able to account for the complex shape deformations, the reorganization of the actin-network, and the coupling to the substrate. As in experiments, we are able to observe preferential alignment along perpendicular, parallel, or oblique angles to the stretching, depending on the frequency of stretching, as well as on the type of response exhibited by our model cells.

arXiv:1807.02295v1 [physics.bio-ph] 6 Jul 2018

* john@cheme.kyoto-u.ac.jp

I. INTRODUCTION

The structure and function of cells is carefully regulated by the signals they receive from their environment. Of particular interest is the transfer of mechanical forces and stresses, which in turn are known to trigger specific biochemical responses inside the cell that can significantly alter their behavior, inducing changes in shape, size, motility modes, reorganization of the cytoskeleton, and even cell proliferation and differentiation[1, 2]. This last example is probably the most striking, given the clear bio-medical applications it promises. Carefully engineered biomaterials should allow us to control stem cell fate decisions, i.e., whether or not they divide or differentiate, and which specific cell lineage is chosen[3]. However, before this is possible, we need to have a clear understanding of the interactions between the cells and the chosen biomaterial. For crawling cells, one of the preferred methods to probe this interaction is to place the cells on an elastic substrate that is being periodically stretched/relaxed along a fixed direction. Studying how the cells respond to this continuous perturbation provides crucial information on its mechanosensing abilities. Early experiments on Fibroblasts[4] and endothelial cells[5, 6], both of which contain stress fibers, found that the cells reorient to align their stress fibers in a direction perpendicular to the stretching. Depending on the type of cell, this can imply both a parallel (fish epidermal keratocytes[7]) or perpendicular (fibroblasts) migration direction. This reorientation of the stress fibers has been linked to the depolymerization and disassembly of parallel fibers[8, 9]. However, while the alignment of the stress fibers is necessary to observe cell reorientation, it is by no means sufficient[8]. Finally, cells without stress fibers, such as HL-60 cells and *Dictyostelium*, have been found to migrate perpendicular to the stretching direction[10–12]. While the specific mechanism responsible for this realignment is cell-specific, and likely to depend on the experimental conditions, it is clear that it involves several general ingredients, closely related to the cells' migration mechanism: the strong shape deformation induced by the stretching, the dynamics of the actin network, the myosin-driven contractility, and the interactions with the substrate.

In this work, we extend an established phase-field model of crawling cells[13] to be able to describe the dynamics over substrates undergoing the type of large amplitude cyclic deformations used in experiments, to study the reorientation dynamics. First, in the absence of any direct coupling with the substrate, such that the cells are passively advected by the imposed deformation, we show that at high enough frequencies cells will always align parallel to the direction of stretching. Then, we introduce a simple response, allowing the adhesions between the cell and the substrate to detach if the rate of extension or compression is too large. Within a suitable frequency range, this results in either a perpendicular or a parallel alignment that is analogous to that observed in experiments. The precise mode of alignment will depend on whether the frequency of the stretching is probing the shape deformation, actin, or focal adhesion dynamics.

II. MODEL

Ever since the pioneering studies of Cahn, Hilliard, and Allen, who introduced phase-field models to study the phase-separation of binary alloys[14–17], phase-field modeling has become one of the preferred methods for physicists and material scientists to describe microstructural dynamics in systems with non-homogenous “phases”. These phases can encode the information of any material property of interest, from a difference in density, orientational order, chemical composition, to differences in the electric or magnetic polarization, thus providing a universal framework with which to study a wide variety of phenomena. Recently, this approach has seen considerable success in biology and medicine. Salient examples include, among others, studies on the morphodynamics of crawling cells[13, 18–21], the immune response to invading pathogens[22], axonal extension of nerve cells[23, 24], and cartilage regeneration[25], as well as tumor growth[26, 27]. In this work, we focus on the mechanosensitivity of crawling cells, and in particular on their ability to sense and respond to mechanical cues from a substrate undergoing cyclic stretching. A phase-field approach is ideally suited for this purpose, as it provides a cell-level description which can take into account the actomyosin based propulsion mechanism, the force transmission to and from the substrate (mediated by the focal adhesion sites), as well as allowing for the large shape deformations caused by the externally applied strain. In addition, this type of modeling can easily scale upward to consider the collective dynamics of multi-cellular systems and confluent tissues[28]. In this section, we will introduce the basic phase-field model of crawling cells that we have adopted, which was originally designed to describe the motion of keratocyte-like fragments over visco-elastic substrates without any global deformation. Then, we define the periodic strain imposed on the substrate, and the extensions to the model that are required to consider crawling under such (large-amplitude) cyclic deformations.

A. Phase-Field Model of Cells on Viscoelastic-Substrates

We adopt the 2D model originally developed by Ziebert and Aranson, which describes each cell using a (non-conserved) order parameter ρ , whose values lie between zero (outside the cell) and one (inside the cell). This allows for an implicit tracking of the boundary, avoiding many of the computational difficulties of related sharp interface methods. A free energy functional $F[\rho]$ is then associated to this order parameter and determines the driving force for its time evolution as

$$\partial_t \rho = -\Gamma \frac{\delta F[\rho]}{\delta \rho} \quad (1)$$

with Γ the mobility coefficient for ρ . This is the so-called ‘‘Model A’’ or time-dependent Ginzburg-Landau model[29]. To lowest order, the free energy functional takes the form

$$F[\rho] = \int [f(\rho) + D_\rho (\nabla \rho)^2] d\mathbf{x} \quad (2)$$

where $f(\rho)$ is the free energy density of the homogeneous system and the term proportional to D_ρ provides a penalty term to the formation of sharp interfaces. The free-energy density is defined to have a double-well form, representing the local stability of the two phases $\rho = 0$ and $\rho = 1$, given by

$$f(\rho) = \int_0^\rho (1 - \rho')(\delta[\rho] - \rho')\rho' d\rho' \quad (3)$$

where the value of δ controls the relative stability of the two. The motility of the cell is modeled by introducing an additional polar order parameter \mathbf{p} , which gives the average orientational order of the actin filament network responsible for the motion. These filaments are continuously polymerizing at the leading edge and pushing against membrane, allowing the cell to extend forward. This requires that the cell be able to transfer the forces to the substrate, something it is able to do because the actin-network is connected to the substrate through the focal adhesion bonds. This is modeled by introducing an additional field A , representing the density of adhesion bonds. Finally, the coupled set of equations for ρ , \mathbf{p} , and A are given by[13]

$$\partial_t \rho = D_\rho \nabla^2 \rho - (1 - \rho)(\delta[\rho] - \rho)\rho - \alpha(A)\nabla \rho \cdot \mathbf{p} \quad (4)$$

$$\partial_t \mathbf{p} = D_p \nabla^2 \mathbf{p} - \tau_1^{-1} \mathbf{p} - \tau_2^{-1} (1 - \rho^2) \mathbf{p} - \beta f[\nabla \rho] - \gamma (\nabla \rho \cdot \mathbf{p}) \mathbf{p} \quad (5)$$

$$\partial_t A = D_A \nabla^2 A + \rho(a_0 \|\mathbf{p}\| + a_{nl} A^2) - (d(u) + sA^2)A \quad (6)$$

where, without loss of generality we have taken $\Gamma = 1$. For the dynamics of ρ (Eq.(4)), the first two terms on the right-hand side result from taking the functional derivative of the energy functional of Eq. (2), while the last term, proportional to $\nabla \rho \cdot \mathbf{p}$ and akin to an advection term, represents the active contribution of the actin-network pushing the cell membrane. The strength with which the actin network can push on the membrane is given as a function of the local density of adhesion sites $\alpha(A)$. The dynamics of \mathbf{p} (Eq.(5)) is given by a simple reaction-diffusion equation, with a source term to account for the polymerization at the interface ($\propto \beta f[\nabla \rho]$), and a decay term ($\propto \tau_1^{-1}$) to account for the corresponding depolymerization. The polymerization is chosen to be a function of the gradient of ρ that ensures that the growth rate is bounded and limited to the interface, with

$$\mathbf{f}[\mathbf{x}] = \frac{\mathbf{x}}{\sqrt{1 + \epsilon \|\mathbf{x}\|^2}} \quad (7)$$

As such, the maximum growth rate is given by $\simeq \beta/\sqrt{\epsilon}$. Note that an additional decay term $\propto \tau_2^{-1}(1 - \rho^2)$ is included for computational simplicity, to make sure that the actin field is non-zero only inside the cell. The last term in Eq. (5) accounts for the myosin induced bundling at the rear of the cells[20], helping to break the $\pm \mathbf{p}$ symmetry and favor polarization. A similar reaction-diffusion model is used for the concentration of adhesion sites A (Eq. (6)). Naturally, the attachment to the substrate can only occur inside of the cell: there is a linear term proportional to $a_0 \|\mathbf{p}\|^2$, since the attachments can only form in the presence of actin, and a non-linear term $a_{nl} A^2$ to model the maturation and growth of existing bonds. For the detachment, there is a linear term that couples the dynamics of A with the substrate displacement u , and a non-linear term that saturates the total number of bonds. The δ function, controlling the relative stability of the two phases is given by ($\langle \cdot \rangle = \int \cdot d\mathbf{r}$)

$$\delta[\rho] = \frac{1}{2} + \mu(\langle \rho \rangle - V_0) - \sigma \|\mathbf{p}\|^2 \quad (8)$$

where the second term on the right hand side acts as a global constraint on the cell volume, and the third term accounts for the myosin-induced contraction.

At first glance, the model can seem overly complex, as it possesses over a dozen free parameters. Fortunately, a detailed analysis of this model and its variants has already been performed[30, 31], allowing us to focus on the few parameters relevant for a study on the mechanosensitivity of cells on periodically stretched substrates. The activity of the cell can be controlled by the strength of the propulsion (α) and the rate of polymerization (β). The shape of the cell can be controlled mainly by the strength of the contractility (σ), with low (high) values resulting in fan(crescent)-like shapes. The motor-asymmetry (γ) has only a small effect on the shape or dynamics of the cell and can be considered constant without loss of generality. Of the remaining parameters appearing in the equations of motion for \mathbf{p} and A , the most important is a_0 , which sets the rate at which new adhesion sites can be formed with the substrate. For example, to consider patterned substrates, one would make this parameter be position dependent. Such a study has been presented in Ref. [13], where a visco-elastic Kelvin-Voigt model is used to describe the displacement of the substrate due to the traction forces exerted by the cell. By controlling just two parameters, the stiffness of the substrate and the rate of attachment (a_0), the authors report a wide variety of motility modes, such as steady gliding motion, stick-slip, bipedal and wandering, which have also been observed experimentally.

B. Substrate Deformation

We consider a substrate that is being cyclically stretched along one of its axes. In most cases, this will necessarily imply a compression along the perpendicular axes, with an amplitude that depends on the Poisson's ratio ν of the material. To describe this deformation, it is convenient to introduce Lagrangian (material) coordinates $\boldsymbol{\xi}$ to label the substrate elements. The time-dependent (Eulerian) coordinates of a given element $\boldsymbol{\xi}$ are then given by $\mathbf{x} = \mathbf{x}(\boldsymbol{\xi}, t)$, which, for the present case is given explicitly by

$$x^1 = (\xi^1 - L_x/2)(1 + \varepsilon(t)) \quad (9)$$

$$x^2 = (\xi^2 - L_y/2)(1 + \varepsilon(t))^{-\nu} \quad (10)$$

where ε is the lateral strain (along which the substrate is being actively deformed), and L_x and L_y are the (undeformed) substrate dimensions. For simplicity, we assume a sinusoidal perturbation given by

$$\varepsilon(t) = \frac{\varepsilon_0}{2}(1 - \cos(2\pi\omega t)) \quad (11)$$

We thus have two equivalent representations for our system, in terms of the body ($\boldsymbol{\xi}$) or lab (\mathbf{x}) frame. Given the time-dependent deformation of the substrate, it is more convenient to solve the equations of motion in the body frame, which is by definition constant, than it is to solve them in the lab frame. Therefore, we must define the appropriate transformations to formulate the problem in the convenient time-independent body frame. This is a common strategy when solving flow or elasticity problems in the presence of time-dependent boundary conditions[32–34]. However, this requires careful consideration, particularly with regards to the definition of the time derivatives.

Let \mathbf{e}_i and \mathbf{E}_I be the basis vectors in the lab and body frame, respectively, and u^i and u^I the corresponding (contravariant) components of a given vector $\mathbf{u} = u^i \mathbf{e}_i = u^I \mathbf{E}_I$. Throughout this work we will assume the Einstein summation convention, and reserve lower (upper) case indices for quantities in the lab (body) frame. The corresponding transformation rules are given by[35]

$$\mathbf{e}_i = \Lambda^I_i \mathbf{E}_I \quad \mathbf{E}_I = \Lambda^i_I \mathbf{e}_i \quad (12)$$

$$u^i = \Lambda^i_I u^I \quad u^I = \Lambda^I_i u^i \quad (13)$$

with $\Lambda^I_i \equiv \partial \xi^I / \partial x^i$, $\Lambda^i_I \equiv \partial x^i / \partial \xi^I$, and $\Lambda^I_i \Lambda^i_J = \delta^I_J$. The inner or scalar product between two vectors is defined as $\mathbf{u} \cdot \mathbf{v} \equiv u_I v^I = u^I v_J = G_{IJ} u^I v^J = G^{IJ} u_I v_J$, with G_{IJ} and G^{IJ} the components of the metric tensor and its inverse ($G^{IJ} G_{JK} = \delta^I_K$)

$$G_{IJ} = \Lambda^i_I \Lambda^j_J g_{ij} = \begin{pmatrix} (1 + \varepsilon(t))^2 & 0 \\ 0 & (1 + \varepsilon(t))^{-2\nu} \end{pmatrix} \quad (14)$$

where the metric tensor in the lab frame is the Euclidean metric tensor $g_{ij} = \delta_{ij}$. For what follows, we will also require the coordinate flow velocity \mathbf{U} , i.e., the velocity of the coordinates or the velocity of the moving substrate. In the body frame, this is defined as[33]

$$\mathbf{U} \equiv -\frac{\partial \boldsymbol{\xi}}{\partial t} = \begin{pmatrix} \tilde{\varepsilon}(\xi^1 - L_x/2) \\ -\nu \tilde{\varepsilon}(\xi^2 - L_y/2) \end{pmatrix} \quad (15)$$

where $\tilde{\varepsilon} = \frac{\varepsilon}{1+\varepsilon}$ and

$$\dot{\varepsilon}(t) = \partial_t \varepsilon(t) = 2\pi\omega \frac{\varepsilon_0}{2} \sin(2\pi\omega t) \quad (16)$$

C. Crawling Cells on Periodically Stretching Substrates

To consider the dynamics of the cell on the periodically stretching substrate, we begin by writing down the equations of motion in contravariant form in the body (substrate) frame of reference, replacing the time-derivatives with intrinsic time derivatives (see Appendix A), to obtain

$$\partial_t \rho = D_\rho \Delta \rho - (1 - \rho)(\delta[\rho] - \rho)\rho - \alpha(A)p^J \nabla_J \rho \quad (17)$$

$$\partial_t p^I = D_p \Delta p^I - \tau_1^{-1} p^I - \tau_2^{-1} (1 - \rho^2) p^I - \beta G^{IJ} \frac{\nabla_J \rho}{1 + \varepsilon \nabla^K \rho \nabla_K \rho} - \gamma (p^J \nabla_J \rho) p^I - p^J \nabla_J U^I \quad (18)$$

$$\partial_t A = D_A \Delta A - \tau_A^{-1} (1 - \rho^2) A + \rho (a_0 p^J p_J + a_{nl} A^2) - (d(\dots) + s A^2) A - A \nabla_J U^J \quad (19)$$

where $\nabla_J \rho = \partial_{\xi^J} \rho = \partial_I \rho$ and $\nabla_J U^I = \partial_J U^I + \Gamma_{KJ}^I U^K$ are the components of the covariant derivative of ρ and U , respectively (Γ_{JK}^I the connection coefficients). In addition, the Laplacian operator ∇^2 is here replaced with the Laplace-Beltrami operator Δ . In the current case, all connection coefficients are zero ($\Gamma_{JK}^I = 0$), considerably simplifying the calculations, since $\Delta \rho = G^{JK} \partial_{\xi^J} \partial_{\xi^K} \rho$ and $\Delta p^I = G^{JK} \partial_{\xi^J} \partial_{\xi^K} p^I$. The final set of equations (17-19) are almost the same as in the original formulation (4-6), except for the last term on the right-hand side of the equations for \mathbf{p} and A , which depend on the gradient of the coordinate flow velocity ($\nabla \mathbf{U}$)

$$\nabla \mathbf{U} \equiv \begin{pmatrix} \nabla_1 U^1 & \nabla_2 U^1 \\ \nabla_1 U^2 & \nabla_2 U^2 \end{pmatrix} = \begin{pmatrix} \tilde{\varepsilon}(t) & 0 \\ 0 & -\nu \tilde{\varepsilon}(t) \end{pmatrix} \quad (20)$$

and an additional decay term (τ_A^{-1}) for the adhesion sites outside the cell. We found the latter to be necessary to avoid any spurious adhesion mediated interactions between the cell and its periodic images, particularly when using small system sizes or frequencies. The precise functional form for the detachment rate d will be discussed in the next subsection. The additional term in the equation for \mathbf{p} comes from the time-dependent nature of the basis vectors, whereas the term appearing in the equation for A comes from the time-dependence of the volume element, and is required to ensure the total conservation of bonds under stretching. Of note is the fact that the equations of motion are now translationally invariant, i.e., there is no explicit dependence on the coordinates ξ . This allows us to assume periodic boundary conditions and employ efficient pseudo-spectral methods to solve the equations. Details on the numerical implementation can be found in Appendix B.

D. Cell-Substrate Coupling

From experiments, we know that cells respond to mechanical stimuli by reorganizing their actin-filament network and distribution of focal adhesion sites. To probe this response, many experiments have focused on studying the reorientation of cells under periodically stretched substrates. Quantitatively, the results are cell-specific, however, several key factors have been identified. In particular, it seems that the actin-filament depolymerization is increased in the direction of stretching, with new filaments assembling at oblique angles[5–9, 36–38], accompanied with a preferential detachment of focal adhesions. While the reorientation of the actin-network is necessary for the reorientation of the cell, it is by no means sufficient, and seems to depend on complicated signaling pathways that are still not completely understood and probably vary among cell types. For example, Hayakawa et al.[8] showed that inhibiting the influx of Ca^{2+} through stress activated ion channels suppressed the reorientation of A10 cells (rat vascular smooth muscle cells), even though the stress-fiber reorientation was not affected. Iwadate et al.[11] found that dyctyostelium cells, which do not possess stress fibers, align perpendicular to the stretching and exhibit a localization of myosin II at the lateral edges of the cell, likely inducing a retraction of the pseudopodia or preventing their extension; while no preferential localization or orientation was observed for actin filaments, at least in the middle of the cell. Finally, while most studies focused on the amplitude dependence, a few recent works[7, 9, 11, 12, 37–39], have considered the frequency dependency for various cell types. In particular, Liu et al.[39] found that the alignment of arterial smooth muscle cells is maximized for a given value of the stretching frequency, and Jungbauer et al.[9] and Greiner et al.[38] both reported a lower threshold frequency below which no alignment is observed. However, the former found that the response time decreased with increasing frequency (above the lower threshold), before plateauing at an upper frequency threshold, whereas the latter found no change in the response time.

We have yet to specify the form of the cell-substrate coupling in our proposed phase-field model. As briefly summarized above, it should depend both on the amplitude of the deformation, as well as on the frequency, and is coupled not just to the rate of polymerization and depolymerization of actin filaments, but the adhesion dynamics and more complicated bio-chemical processes taking place inside the cell. However, for simplicity, within the current phenomenological description, we consider that the coupling to the substrate comes purely from the adhesion dynamics, in the form of a strain dependent detachment rate. Since we wish to study the frequency dependent response, we assume that the detachment rate is sensitive only to the rate at which the substrate is being stretched. In a more detailed model, we could consider that this detachment rate would depend also on the relative alignment of the actin-filaments, as well as include a rate-dependent polymerization or depolymerization rate. This will be left for future work.

As an objective measure of the rate at which the substrate is stretching, we use the (Lagrangian) rate of deformation tensor D , defined as the time-derivative of the Green deformation tensor (or the right Cauchy-Green tensor), which in component form is given by[40]

$$2D^I{}_J = G^{KI} g_{ik} \left(\Lambda^i{}_J \nabla_K U^k + \Lambda^k{}_K \nabla_J U^i \right) \quad (21)$$

In Eulerian terms, it yields the symmetric part of the velocity gradient tensor, and, as its name suggests, it provides information on the rate at which an object is being deformed or stretched. We consider that the rate of detachment d depends solely on the trace of this rate of deformation tensor $D = \text{tr } D$, i.e., how fast it is being stretched or compressed. Furthermore, given the experimental findings of a lower-frequency threshold, we assume a sharp sigmoidal response, such that $d = 0$ ($d = 1$) below (above) the critical frequency ω_c . We introduce three basic response function

$$d^{(\pm)}(D) = \frac{d}{2} \left[1 + \tanh \left(b^2 (D^2 - D_c^2) \right) \right] \quad (22)$$

$$d^{(+)}(D) = \frac{d}{2} \left[1 + \tanh \left(b^2 (R^2(D) - D_c^2) \right) \right] \quad (23)$$

$$d^{(-)}(D) = \frac{d}{2} \left[1 + \tanh \left(b^2 (R^2(-D) - D_c^2) \right) \right] \quad (24)$$

with D_c the critical deformation rate, $R(x) = xH(x)$ the ramp function (H the Heaviside step function), and b a numerical parameter to control the stiffness of the response. Thus, cells can respond to both expansion and contraction ($d^{(\pm)}$), only to expansion ($d^{(+)}$), or only to contraction ($d^{(-)}$). In all cases, when $d = 1$, attachments to the substrate will break, which will lead to a cell that stops moving, since the propulsion term depends linearly on A , and tries to recover its circular shape.

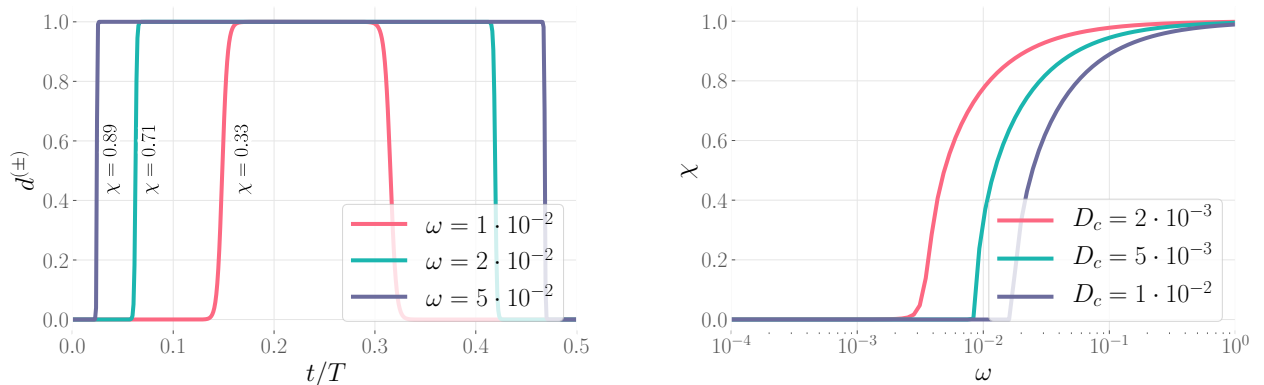


FIG. 1. (left) Detachment rate as a function of time for three different frequencies, with $D_c = 5 \cdot 10^{-3}$, $b = 10^3$, and $d = 1$. (right) Average detachment rate χ , as a function of frequency, for three different critical stretching rates D_c .

Assuming a step-like response, which is a good approximation if b is large enough, $d = 1$ for $D^2 - D_c^2 \geq 0$, then leads to the following quadratic equation for $y = 1 - \cos(2\pi\omega t)$, from which we can estimate the critical frequency ω_c

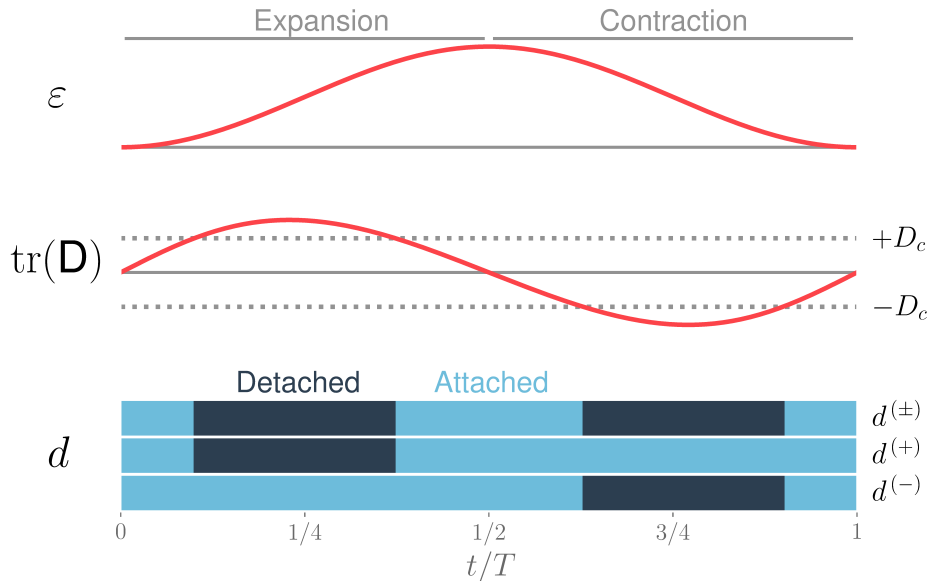


FIG. 2. Schematic Representation for the adhesion/substrate coupling. From top to bottom, the stretch ratio ε , the trace of the rate-of-deformation tensor $D = \text{tr}(D)$, and the magnitude of the detachment rate $d(D)$ for three different response functions: expansion-contraction $d^{(\pm)}$, expansion $d^{(+)}$, and contraction $d^{(-)}$.

as a function of D_c

$$B^2 = \frac{y(2-y)}{\left(1 + \frac{\varepsilon_0}{2}y\right)^2} \quad (25)$$

with $B = \frac{D_c}{\pi\omega\varepsilon_0(1-\nu)}$. The roots to this equation are given by

$$\left(1 + (B\varepsilon_0/2)^2\right) \cos(2\pi\omega t) = B^2 \frac{\varepsilon_0}{2} \left(\frac{\varepsilon_0}{2} + 1\right) \pm \sqrt{1 - B^2(1 + \varepsilon_0)} \quad (26)$$

and are real only if the term inside the square root is greater than zero, from which we can derive the critical frequency

$$\omega_c = \frac{D_c}{\varepsilon_0(1-\nu)\pi} \sqrt{1 + \varepsilon_0} \quad (27)$$

Finally, to quantify the degree to which this detachment rate affects the dynamics, we define a function χ that measures the average detachment rate over a half-cycle

$$\chi = \frac{2}{dT} \int_{t_0}^{t_0+T/2} d^{(\alpha)}(D(t)) dt \quad (28)$$

Alternatively, this also provides a measure of the relative time-interval during which the cell can move. Fig. 1 shows the detachment rate as a function of time, as well as the average detachment rate as a function of frequency, Fig. 2 gives a schematic diagram of the three main quantities involved in determining the response of the cell: the time-dependent strain, the rate of deformation D , and the detachment rate $d(D)$.

III. RESULTS

We consider a single cell on a periodically-stretched substrate, at various frequencies, and study the time-dependent orientation for the three different response functions introduced above $d^{(\pm)}$, $d^{(+)}$, and $d^{(-)}$. As a reference, we have also considered the case when $d = 0$, as it serves to identify to what degree the reorientation can be attributed to the

Parameter	Value	Description
α	4	Propulsion rate
β	$\alpha/2$	Actin nucleation rate
γ	0.5	Motors' symmetry breaking
σ	1.3	Motors' contraction
μ	0.1	Stiffness of volume conservation
D_ρ	1	Stiffness of the diffuse interface
D_p	0.2	Diffusion coefficient for \mathbf{p}
τ_1^{-1}	0.1	Degradation rate of actin
τ_2^{-1}	0.4	Decay rate of \mathbf{p} outside of cell
ϵ	37.25	Regularization of actin creation
D_A	1	Diffusion of adhesion sites
a_0	0.01	Linear adhesion attachment rate
a_{nl}	1.5	Nonlinear adhesion attachment rate
s	1	Saturation of adhesion sites
d	1	Adhesion detachment rate
τ_A^{-1}	τ_2^{-1}	Decay rate of adhesion sites outside of cell
ν	0.3	Poisson ratio
ω	0 – 0.1	Substrate Stretching frequency
ϵ_0	0.3	Substrate deformation amplitude
D_c	$10^{-3} - 10^{-1}$	Critical rate-of-deformation
b	10^3	Stiffness parameter for detachment rate response
r_0	15	Radius of circular initial condition

TABLE I. Simulation parameters.

passive deformation of the cell by the substrate. Since our stated interested is to consider the frequency dependence of the cell dynamics, we have fixed all parameters related to the cell and substrate. Unless otherwise stated, the default values are those listed in Table I, which were taken from a previous study on patterned substrates performed by Ziebert and Aranson[13]. In the absence of stretching, a polarized cell with these parameters will settle into a steady gliding motion with a fan-like shape. Regarding the stretching protocol, we follow the experiments of Iwadate et al[10], and set the Poisson's ratio at $\nu = 0.3$, with a fixed amplitude of $\epsilon_0 = 0.3$. For all simulations we considered a single cell of circular radius $r_0 = 15$, that was initially polarized at an angle θ with respect to the stretching direction ($\theta = 0$). The initial values for the magnitude of the polarization field and the concentration of adhesion sites were set to $p = 0.5$ and $A = 0.1$, respectively. The dimensions of the (unstretched) domain were $L_x = L_y = 100$ and we used $N = 256$ grid points along each dimension to discretize the system.

To track the orientation of the cells, we computed the center of mass as a function of time and from this, the (relative) center of mass velocity, within the lab frame, was obtained and used to define θ . Specifically, let $\Delta\mathbf{r}(t_0, t_1) = \mathbf{r}(t_1) - \mathbf{r}(t_0)$ be the center of mass displacement, within the lab frame, in a time interval $\Delta t = t_1 - t_0$. To compute the relative velocity of the cell \mathbf{v}_{eff} with respect to the substrate we should remove the displacement corresponding to the externally imposed strain. Consider a substrate element that at time $t = t_0$ coincides exactly with the position of the center of mass $\mathbf{r}(t_0)$. The Lagrangian coordinates for this element are $\boldsymbol{\xi}(\mathbf{r}(t_0), t_0)$. The spatial position of this element at any subsequent time t_1 is known exactly, since it follows the substrate deformation, and allows us to define the effective substrate velocity $\mathbf{u}(t_0, t_1)$ as

$$\mathbf{u}(t_0, t_1) = \frac{\mathbf{x}(\boldsymbol{\xi}(\mathbf{r}(t_0), t_0), t_1) - \mathbf{r}(t_0))}{\Delta t} \quad (29)$$

Thus, the effective velocity of the cell, within the reference frame of the lab is simply

$$\mathbf{v}_{\text{eff}}(t_0, t_1) = \frac{1}{\Delta t} \left[\Delta\mathbf{r}(t_0, t_1) - \Delta t \mathbf{u}(t_0, t_1) \right] \quad (30)$$

To obtain accurate measurements for \mathbf{u}_{eff} we made sure that the sampling time Δt was smaller than both the period of oscillation ($T = \omega^{-1}$) and the time τ required for the cell to move a distance equal to its diameter (at $\omega = 0$).

To understand the reorientation dynamics, we need to consider the interplay between the dynamics of the shape deformations, the actin dynamics, and the adhesion dynamics, as well as their characteristic time-scales, and how

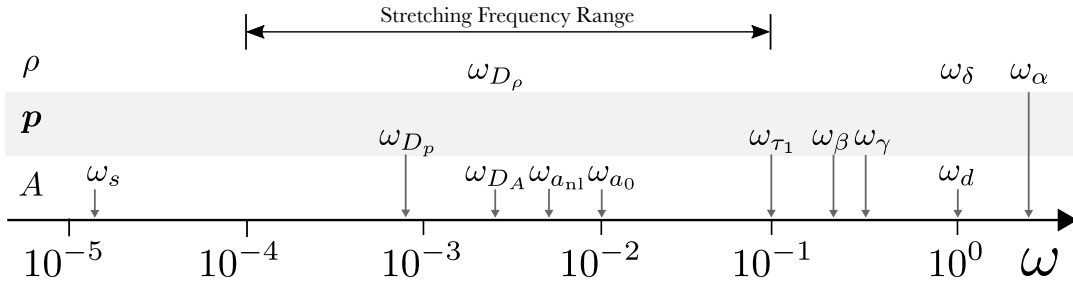


FIG. 3. Relevant time/frequency scales for the cell ρ , polarization \mathbf{p} , and adhesion A dynamics.

they compare to the time-scale over which the substrate is being deformed. For this we first define the characteristic length scales in the system, the cell size $r_0 = 15$ and the interface thickness $\zeta = D_\rho^{1/2} = 1$. The characteristic time or frequency of the shape deformations is determined by the stiffness of the interface as $\omega_{D_\rho} = D_\rho r_0^{-2} \simeq 4 \cdot 10^{-3}$, as well as the time governing the retraction/expansion of the two phases $\omega_\delta = 1$. The frequency associated to the propulsion of the cell by the actin network is $\omega_\alpha = \alpha \zeta^{-3} \simeq 4$. The time-scales for the actin dynamics include the diffusion time-scale D_p , the depolymerization rate (τ_1), the polymerization rate (β), and the asymmetry driving term (γ). They in turn yield the following characteristic frequencies, $\omega_{D_p} = D_p r_0^{-2} \simeq 9 \cdot 10^{-4}$, $\omega_{\tau_1} \simeq \tau_1^{-1} = 10^{-1}$, $\omega_\beta = \beta \epsilon^{-1/2} \simeq 3 \cdot 10^{-1}$, and $\omega_\gamma = \gamma \zeta^{-1} \simeq 5 \cdot 10^{-1}$. Finally, the frequencies associated to the adhesion dynamics are $\omega_{D_A} = D_A r_0^{-2} \simeq 4 \cdot 10^{-3}$, $\omega_{a_0} = a_0 \zeta^2 = 10^{-2}$, $\omega_{a_{nl}} = a_{nl} r_0^{-2} \simeq 7 \cdot 10^{-3}$, $\omega_s = s r_0^{-4} \simeq 2 \cdot 10^{-5}$, and $\omega_d = d = 1$. Where it should be noted that the relevant length scale for the linear attachment rate is the interface width ζ , as this is where the polarization \mathbf{p} field is concentrated, whereas that for the non-linear growth and saturation rates is the cell size r_0 . To summarize, we can identify the following regimes governing the shape, actin, and adhesion dynamics

$$\begin{aligned} \omega_{D_\rho} &\ll \omega_\delta < \omega_\alpha \\ \omega_{D_p} &\ll \omega_\gamma < \omega_{\tau_1} < \omega_\beta \\ \omega_s &\ll \omega_{D_A} < \omega_{a_{nl}} < \omega_{a_0} \ll \omega_d \end{aligned}$$

An illustration of the different frequency regimes is given in Fig. 3. Here, we will focus on stretching frequencies within the range $10^{-4} < \omega < 10^{-1}$, so the relevant time scales are between ω_{D_p} and ω_{a_0} .

A. Passive alignment

Let us start by considering the simple case of a cell that is being passively advected by the substrate, in the absence of any direct coupling with the substrate, i.e., $d = 0$. The results for this case are summarized in Fig. 4, which shows the orientation as a function of time, for various stretching frequencies ω . For $\omega = 0$, the orientation of the cell is time-independent, as expected. For non-zero frequencies, the orientation shows a clear time-variation, since it is being constantly deformed and rotated by the substrate. However, there are several distinct frequency regimes, depending on how the stretching frequency compares to the characteristic frequencies of the system, giving rise to qualitatively different realignment dynamics. At very low frequencies, $\omega \lesssim 10^{-4}$, the orientation oscillates around the initial value, but there is no stretch-induced alignment. In this case, the deformation is so slow that the cell (together with the actin network and adhesion sites) can completely follow the imposed strain. As the frequency is increased further, such that it becomes comparable to the frequency for the diffusion of orientational order ω_{D_p} , we begin to see an alignment either parallel or perpendicular to the stretching direction. In this case, the actin network is not able to rearrange fast enough to adapt to the changing shape of the cell. However, this alignment is extremely slow, with a time-scale of the order of $t/\tau \simeq 10^4$. In addition, there seems to be no preference between parallel or perpendicular directions, with the final orientation depending only on the initial orientation. Cells that were aligned closer to the parallel or perpendicular directions will favor those orientations. Upon increasing the frequency of oscillation to $\omega \simeq 5 \cdot 10^{-3}$, the qualitative behavior remains unchanged, but the reorientation time-scale is significantly reduced, by roughly an order of magnitude. At these frequencies, the substrate is stretching faster than the cell can relax, since $\omega > \omega_{D_p}$, so that the shape is strongly perturbed by the imposed strain. If the frequency is increased still further, we observe a clear transition, at $\omega \simeq 2 \cdot 10^{-2}$, above which all cells show a parallel alignment, regardless of the initial orientation. The reason for this realignment is the fact that new adhesion bonds cannot formed fast enough to keep track of the deformation, as $\omega > \omega_{a_0} > \omega_{a_{nl}}$.

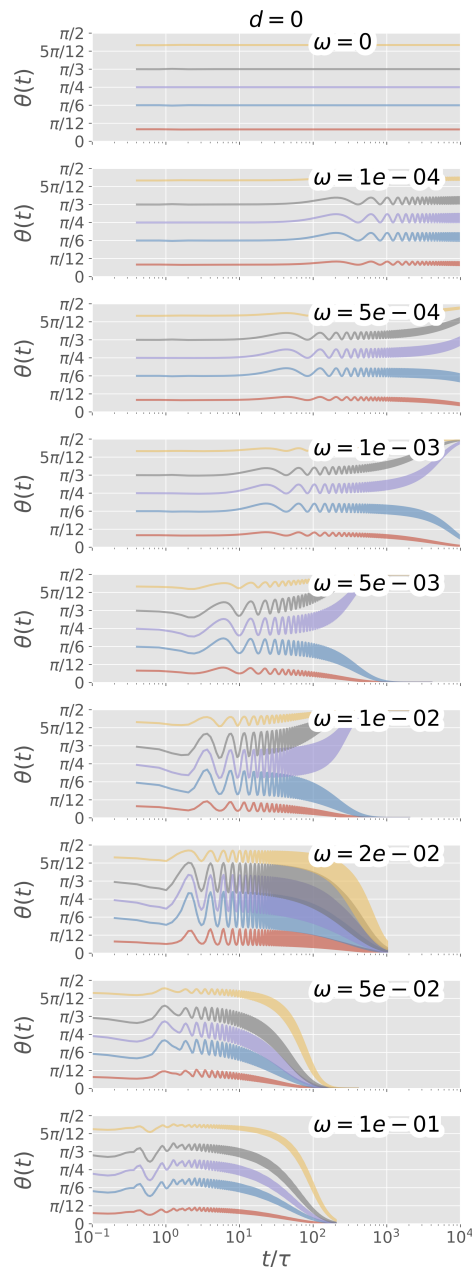


FIG. 4. Orientation θ as a function of time t for various frequencies, in the absence of any specific cell-substrate coupling ($d = 0$).

Even without any specific cell-substrate interaction, the strong coupling that exists between shape and motility yields a preferential alignment under cyclic stretching that is strongly dependent on the relative frequency. At very low frequencies the cells and the actin network have time to readjust to the deformation, and the average migration direction is not affected. When the stretching is faster than the actin network can respond to, there is a very weak reorientation process, but no preference between perpendicular or parallel directions. If the stretching is faster than the time-scale over which the cell can accommodate its shape (as defined by the stiffness of the membrane), then the reorientation is significantly faster. At even higher frequencies, where the creation of new adhesion bonds is not fast enough to follow the deformation, we observe that the cells align parallel to the stretching direction, regardless of initial orientation. Thus, even in the absence of any direct coupling to the substrate, there is a clear preference in the migrating direction, simply due to the coupling between shape and motility.

B. Active alignment

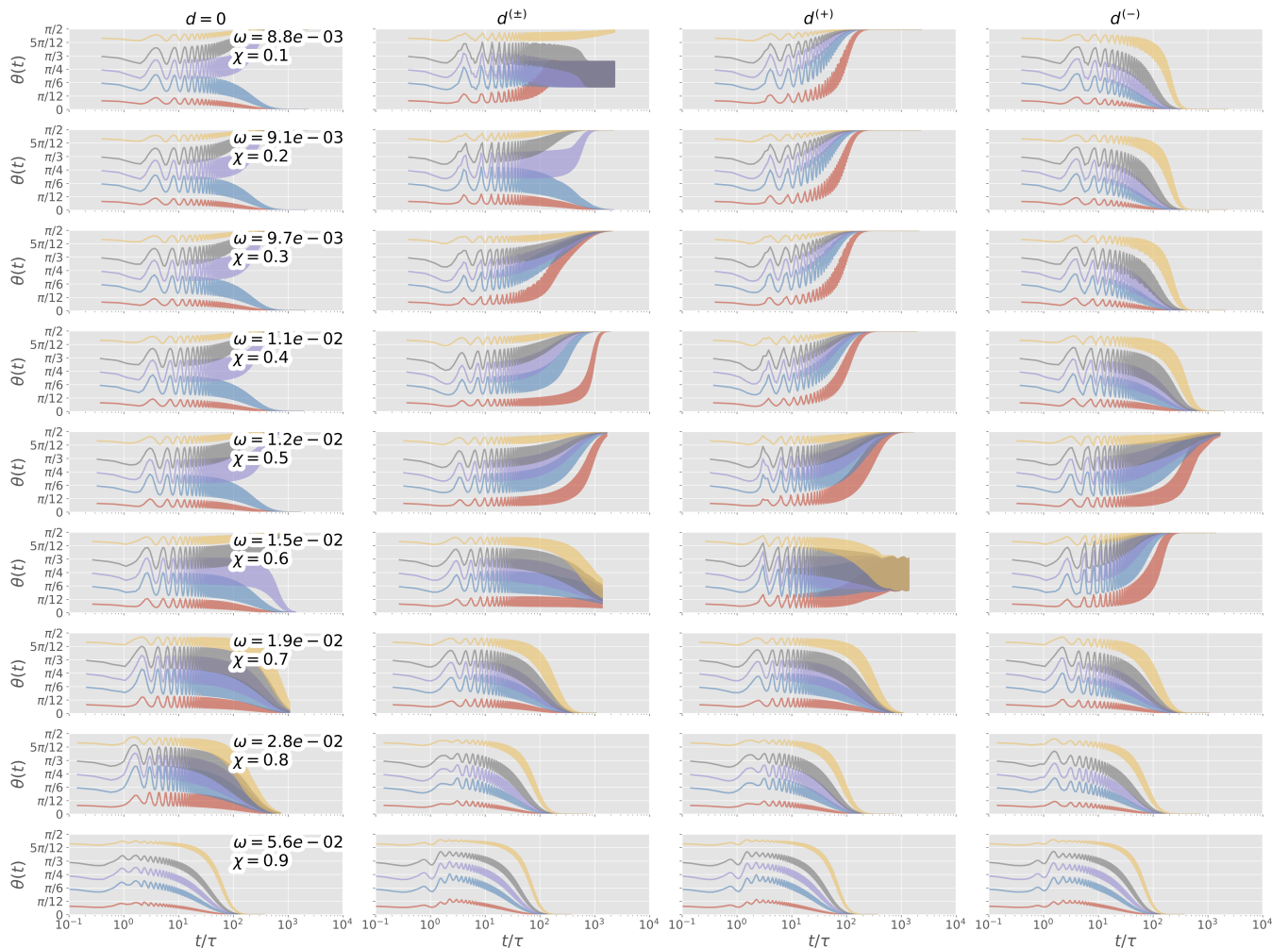


FIG. 5. Orientation θ as a function of time t for various frequencies and adhesion response functions. The critical stretching rate was $D_c = 5 \cdot 10^{-3}$.

We now consider the reorientation of cells whose internal propulsion mechanism is actively responding to the strain it receives from the substrate through a rate-dependent detachment rate ($d \neq 0$). As described above, we will consider cells that respond to either compression $d^{(-)}$ or extension $d^{(+)}$, or both $d^{(\pm)}$. By setting the threshold value D_c (ω_c) at which this response is activated, we can control the interval during which the cell is able to form attachments, and thus crawl over the substrate. Taking into account the results presented above in the absence of any direct coupling $d = 0$, for which the cells show parallel reorientation when the frequency of oscillation is greater than the frequency associated to the attachment dynamics, a rate-dependent detachment rate will significantly affect the reorientation dynamics. Simulation results for $D_c = 5 \cdot 10^{-3}$, with a corresponding critical frequency of $\omega_c \simeq 8 \cdot 10^{-3} \lesssim \omega_{a_0}$, are summarized in Fig. 5, for a range of frequencies $8 \cdot 10^{-3} < \omega < 6 \cdot 10^{-2}$ (χ between 0 and 1). Within this frequency range, the only relevant time scales are those corresponding to the attachment dynamics $\omega_{a_{n1}}$ and ω_{a_0} , as the relevant time scales for the actin and shape deformations are both slower $\omega_{D_\rho} < \omega_{D_\rho} < \omega$. For these lower frequencies $d = 0$ and the reorientation dynamics would be the same as in the passive case. For comparison purposes, the corresponding results for $d = 0$ have also been included. Looking at the high frequency response ($\omega \gtrsim 2 \cdot 10^{-2}$), we see that all cell types show parallel alignment, regardless of the specific form of the response function. In such cases, the stretching is too fast for the cell to respond ($\omega > \omega_{a_0} > \omega_\rho > \omega_p$), so the specific details of the detachment dynamics become irrelevant. More interesting are the results at low and intermediate frequencies. At low frequencies $8 \cdot 10^{-3} \lesssim \omega \lesssim 1.1 \cdot 10^{-2}$ ($0.1 \leq \chi \leq 0.4$), cells with $d^{(+)}$, which “resist” extension, exhibit a perpendicular alignment. In contrast, cells with $d^{(-)}$, which “resist” compression, show a parallel alignment within the same frequency range.

It is clear that this alignment is due to the type of detachment, since cells with $d = 0$ show no preferential alignment, with $\theta = 0$ or $\theta = \pi/2$ equally likely. Furthermore, the realignment of the cells with non-zero detachment rate occurs over time-scales that are considerably shorter than those for which $d = 0$. Within this frequency range the cyclic detachments occur at time-scales comparable to the time it takes for the cell to form and grow new attachments. For intermediate frequencies $\omega \simeq \omega_{a_0}$, with $\chi \simeq 0.5$, $d^{(+)}$ cells exhibit a transition between the low frequency response (favoring perpendicular orientations) and the high frequency response (favoring parallel orientations), resulting in a stable oblique orientation $\theta \simeq \pi/4$. Surprisingly, the $d^{(-)}$ cells also exhibit a non-monotonic behavior, even though the low and high frequency limits both show parallel orientations, at $\omega \simeq 1.2 \cdot 10^{-2}$ ($\chi \simeq 0.5$) cells align perpendicular to the stretching direction. The behavior of the $d^{(\pm)}$ cells seems more complicated, but it can roughly be understood as a competition the opposing tendencies of $d^{(+)}$ and $d^{(-)}$ cells to orient perpendicular or parallel to the stretching at low frequencies, with the perpendicular response being dominant. This is consistent with the fact that the reorientation time-scale is much slower than that of the other cell types.

We have performed simulations for two other critical stretching rates, $D_c = 2 \cdot 10^{-3}$ ($\omega_c \simeq 3 \cdot 10^{-3}$) and $D_c = 10^{-2}$ ($\omega_c \simeq 10^{-2}$), and found similar behavior, at least in the high frequency range. However, for $\omega_c = 3 \cdot 10^{-3} \lesssim \omega_{D_\rho} = 4 \cdot 10^{-3}$, the stretching is now able to probe the shape-deformations. For the lowest frequency considered, $\omega = 3.4 \cdot 10^{-3}$ ($\chi = 0.1$), the $d^{(+)}$ ($d^{(-)}$) cells actually favor a parallel (perpendicular) alignment. Increasing the frequency to $\omega = 3.7 \cdot 10^{-3} \simeq \omega_{D_\rho}$ the system reverts back to being dominated by the adhesion dynamics, thus, if the frequency is not too high $d^{(+)}$ ($d^{(-)}$) cells will tend to align perpendicular (parallel) to the direction of stretching. We note however that for $d^{(-)}$ cells the reorientation response is less pronounced, particularly at intermediate frequencies. At high enough frequencies $\omega > \omega_{a_0}$ all cells show parallel alignment.

IV. CONCLUSIONS

We have developed a cell-level model for crawling cells over periodically stretching substrates that takes into account the large shape deformations induced by the stretching, as well as the internal processes responsible for the motility and coupling to the substrate, i.e., the actin based propulsion mechanism and the focal adhesions with which the momentum is transferred to the substrate. While we have only considered an idealized description of the cell-substrate coupling, in which the adhesions detach if the rate of extension or compression exceeds some threshold, we are able to obtain a non-trivial reorientation of the cells that has been reported in experiments. In the current case, depending on whether the cells stop crawling under too large extension or compression, and how the stretching frequency compares to the characteristic frequencies associated to the shape deformation and the actin and adhesion dynamics, we can observe both perpendicular or parallel alignment, as well as oblique orientations. We find that cells that resist extension will usually align perpendicular to the direction of stretching, at least for moderate frequencies ($\omega \lesssim \omega_{a_0}$). In contrast, cells that resist extension are more likely to favor a parallel orientation. At high enough frequencies all cells align parallel to the direction of stretching.

The question of cellular realignment under the type of periodic stretching considered here has attracted much attention recently due to its biological significance. Indeed, several theoretical and simulation works have managed to provide qualitative agreement with experimental results. Of these, the most relevant for our purposes are the theories of De and Safran[41–43], using an elastic force dipole model, and that of Gao et al.[44–46], using a cytoskeletal tensegrity model. The latter in particular, in which cells are modeled as a series of interconnected bars and strings supporting tensile and/or compressive forces, provides broad quantitative agreement with experiments. However, such effective mechanical descriptions are too simple to accurately account for the detailed coupling between the complex shape deformations and the internal machinery of the cell (e.g., the acto-myosin or adhesion dynamics), as well as its interactions with the underlying substrate. The phenomenological model we propose here provides a cell-level description that is able to account for a wide variety of motility modes seen experimentally and can be easily extended. In future work we will consider in more detail the coupling between the cell and the substrate, in order to provide a more realistic description and show better agreement with experiments.

ACKNOWLEDGMENTS

JJM would like to acknowledge fruitful discussions with Natsuhiko Yoshinaga, Koichiro Sadakane, Kenichi Yoshikawa, Matthew Turner, and Takashi Taniguchi during the preparation of this manuscript. This work was supported by the Japan Society for the Promotion of Science (JSPS) Wakate B (17K17825) and KAKENHI (26247069) grants.

Appendix A: Intrinsic Time Derivatives and Conservation Laws

To modify the equations of motion of the crawling cell for the case where the substrate itself is being stretched, we need to carefully translate the formulas to a time-dependent (non-orthonormal) coordinate system. For the spatial gradient operators, we simply replace partial derivatives (∂_{x^i}) with covariant derivatives (∇_i), however, the main issue here is how to handle the time derivatives. The material derivative should not be used, as it does not yield proper tensorial quantities. Instead, the intrinsic time-derivative should be employed[33, 47]. It defines tensorial quantities that provide the appropriate time-variation of arbitrary grade tensors along particle paths in time-dependent curvilinear coordinates. For scalars (a) and vectors (b^i), this intrinsic time-derivative takes the following form

$$\frac{\delta a}{\delta t} = \partial_t a + (u^k - U^k)\nabla_k a \quad (\text{A1})$$

$$\frac{\delta b^i}{\delta t} = \partial_t b^i + (u^k - U^k)\nabla_k b^i + b^k \nabla_k U^i \quad (\text{A2})$$

where u^k refers to the k -component of the ‘‘particle’’ velocity, U^k to that of the coordinate-flow (i.e., the coordinate-flow velocity of the moving grid), and $\nabla_k a = \partial_k a$ and $\nabla_k b^i = \partial_k b^i + \Gamma_{jk}^i b^j$ are the components of the covariant derivatives (Γ_{jk}^i the connection coefficients). In this work, given the nature of the deformation we are interested in, all connection coefficients are zero. However, as the body basis vectors are not orthonormal, since their length is changing in time, we do need to differentiate between vectors and 1-forms, or contravariant and covariant components.

Thus, we see that the advection terms are proportional to the relative velocity ($\mathbf{u} - \mathbf{U}$). In addition, if $\mathbf{U} = 0$, which corresponds to time-independent coordinates, we recover the standard material derivative $D_t \mathbf{a} = \partial_t \mathbf{a} + \mathbf{u} \cdot \nabla \mathbf{a}$. In this work, we consider the special case $\mathbf{u} = \mathbf{U}$, for which the advection term is exactly zero. This corresponds to an idealized situation of a deformable, yet inelastic substrate. That is, we impose the large-scale deformation of the substrate and ignore any deviations caused by the traction forces exerted by the cell (as these are assumed to be much smaller).

The intrinsic time-derivatives allow us to compute the change in tensorial quantities along particles paths in time-dependent curvilinear coordinates. However, when formulating conservation laws, we must consider the time-variation of extensive (integrated) material quantities. This is given by the Reynolds transport theorem. Consider the total amount of a carried by a given material element, which may be deforming in time. The total change in a is defined as[33]

$$\frac{d}{dt} \int_{V(t)} a \sqrt{g} d\xi^n = \int_{V(t)} \left(\frac{\delta a}{\delta t} + a \nabla_k u^k \right) \sqrt{g} d\xi^n \quad (\text{A3})$$

where $V(t)$ is the (time-dependent) domain of the material element under consideration, \mathbf{u} its velocity, and $g = |\det g_{ij}|$ is the determinant of the metric tensor.

Appendix B: Numerical Implementation

We outline the numerical method used to solve Eqs. (17-19). The differential equations are all of the form

$$\partial_t u = \mathcal{L}(t)u + \mathcal{G}(u, t) \quad (\text{B1})$$

where \mathcal{L} is a linear operator, which can depend on time, but is independent of u , while \mathcal{G} is the non-linear term. Applying an Euler scheme in time, treating the linear part implicitly, and the non-linear part explicitly, we have

$$\frac{u_{n+1} - u_n}{h} = \eta L_{n+1} u_{n+1} + (1 - \eta) L_n u_n + G_n \quad (\text{B2})$$

$$u_{n+1} = \left(1 - h\eta L_{n+1} \right)^{-1} \left(u_n + h[(1 - \eta)L_n u_n + G_n] \right) \quad (\text{B3})$$

where $u_n = u(t_n)$, $L_n = \mathcal{L}(t_n)$, and $G_n = \mathcal{G}(u_n, t_n)$, with h the time step and $t_n = nh$. Choosing $\eta = 0$, corresponding to an explicit calculation of the linear operator, yields

$$u_{n+1} = u_n + h[L_n u_n + G_n] \quad (\text{B4})$$

whereas $\eta = 1$, corresponding to an implicit treatment, results in

$$u_{n+1} = \left(1 - hL_{n+1} \right)^{-1} \left(u_n + hG_n \right) \quad (\text{B5})$$

We use the latter due to its improved stability. To resolve the differential operators, we employ a pseudo-spectral method[48, 49], solving the equation of motion in Fourier space, but computing all non-linear terms in real space and then transforming to Fourier space. For the equations we have considered, the linear operator is usually just the diffusion term $L \propto \Delta u$, which in Fourier space is just $\hat{L} \propto \|k\|^2 \hat{u} = G^{IJ} k_I k_J \hat{u}$ (with k the wave-vector). Fourier transforms were performed using the Fast Fourier Transform, with a typical grid size of 256×256 points on a square domain of size $L = 100$.

-
- [1] P. A. Janmey and C. A. McCulloch, Annual Review of Biomedical Engineering **9**, 1 (2007).
- [2] S. W. Crowder, V. Leonardo, T. Whittaker, P. Papatianasiou, and M. M. Stevens, Cell Stem Cell **18**, 39 (2016).
- [3] V. V. Hiew, S. F. B. Simat, and P. L. Teoh, Stem Cell Reviews and Reports **14**, 43 (2018).
- [4] R. C. Buck, Experimental Cell Research **127**, 470 (1980).
- [5] P. C. Dartsch and E. Betz, Basic Research in Cardiology **84**, 268 (1989).
- [6] T. Iba and B. E. Sumpio, Microvascular Research **42**, 245 (1991).
- [7] C. Okimura and Y. Iwadate, Cell Adhesion and Migration **10**, 406 (2016).
- [8] K. Hayakawa, N. Sato, and T. Obinata, Experimental Cell Research **268**, 104 (2001).
- [9] S. Jungbauer, H. Gao, J. P. Spatz, and R. Kemkemer, Biophysical Journal **95**, 3470 (2008).
- [10] Y. Iwadate and S. Yumura, BioTechniques **47**, 757 (2009).
- [11] Y. Iwadate, C. Okimura, K. Sato, Y. Nakashima, M. Tsujioka, and K. Minami, Biophysical Journal **104**, 748 (2013).
- [12] C. Okimura, K. Ueda, Y. Sakumura, and Y. Iwadate, Cell Adhesion and Migration **10**, 331 (2016).
- [13] J. Löber, F. Ziebert, and I. S. Aranson, Soft Matter **10**, 1365 (2014).
- [14] J. W. Cahn and J. E. Hilliard, The Journal of Chemical Physics **28**, 258 (1958).
- [15] J. W. Cahn, Acta Metallurgica **9**, 795 (1961).
- [16] S. Allen and J. Cahn, Acta Metallurgica **20**, 423 (1972).
- [17] S. M. Allen and J. W. Cahn, Scripta Metallurgica **7**, 1261 (1973).
- [18] D. Shao, W.-J. Rappel, and H. Levine, Physical Review Letters **105**, 108104 (2010).
- [19] D. Shao, H. Levine, and W.-J. Rappel, Proceedings of the National Academy of Sciences **109**, 6851 (2012).
- [20] F. Ziebert, S. Swaminathan, and I. S. Aranson, Journal of The Royal Society Interface **9**, 1084 (2012).
- [21] B. Palmieri, Y. Bresler, D. Wirtz, and M. Grant, Scientific Reports **5**, 1 (2015).
- [22] S. Najem and M. Grant, Soft Matter **10**, 9715 (2014).
- [23] S. Najem and M. Grant, EPL (Europhysics Letters) **102**, 16001 (2013).
- [24] T. Takaki, K. Nakagawa, Y. Morita, and E. Nakamachi, Mechanical Engineering Journal **2**, 15 (2015).
- [25] A. Yun, S. H. Lee, and J. Kim, Bulletin of Mathematical Biology **75**, 2389 (2013).
- [26] G. Sciumè, S. Shelton, W. G. Gray, C. T. Miller, F. Hussain, M. Ferrari, P. Decuzzi, and B. A. Schrefler, New Journal of Physics **15** (2013), 10.1088/1367-2630/15/1/015005.
- [27] E. A. B. F. Lima, J. T. Oden, and R. C. Almeida, Mathematical Models and Methods in Applied Sciences **24**, 2569 (2014).
- [28] J. Löber, F. Ziebert, and I. S. Aranson, Scientific Reports **5**, 1 (2015).
- [29] P. M. Chaikin and T. C. Lubensky, *Principles of condensed matter physics*, 1st ed. (Cambridge University Press, New York, 1995).
- [30] I. S. Aranson, ed., *Physical Models of Cell Motility* (Springer, Cham, 2016).
- [31] F. Ziebert and I. S. Aranson, npj Computational Materials **2**, 1 (2016).
- [32] H. Luo and T. R. Bewley, Journal of Computational Physics **199**, 355 (2004).
- [33] D. Venturi, Journal of Physics A: Mathematical and Theoretical **42** (2009), 10.1088/1751-8113/42/12/125203.
- [34] J. J. Molina, K. Otomura, H. Shiba, H. Kobayashi, M. Sano, and R. Yamamoto, Journal of Fluid Mechanics **792**, 590 (2016).
- [35] B. F. Schutz, *Geometrical methods of mathematical physics*, 1st ed. (Cambridge University Press, Cambridge, 1980).
- [36] J. H.-C. Wang, P. Goldschmidt-Clermont, J. Wille, and F. C.-P. Yin, Journal of Biomechanics **34**, 1563 (2001).
- [37] C.-F. Lee, C. Haase, S. Deguchi, and R. Kaunas, Biochemical and Biophysical Research Communications **401**, 344 (2010).
- [38] A. M. Greiner, H. Chen, J. P. Spatz, and R. Kemkemer, PLoS ONE **8**, e77328 (2013).
- [39] B. Liu, M.-J. Qu, K.-R. Qin, H. Li, Z.-K. Li, B.-R. Shen, and Z.-L. Jiang, Biophysical Journal **94**, 1497 (2008).
- [40] J. E. Marsden and T. J. R. Hughes, *Mathematical Foundations of Elasticity*, 1st ed. (Dover Publications, Inc., New York, 1994).
- [41] R. De, A. Zemel, and S. A. Safran, Nature Physics **3**, 655 (2007).
- [42] S. A. Safran and R. De, Physical Review E - Statistical, Nonlinear, and Soft Matter Physics **80**, 060901 (2009).
- [43] R. De, A. Zemel, and S. A. Safran, Biophysical Journal **94**, L29 (2008).
- [44] J. Qian, H. Liu, Y. Lin, W. Chen, and H. Gao, PLoS ONE **8**, e65864 (2013).
- [45] G.-K. Xu, B. Li, X.-Q. Feng, and H. Gao, Biophysical journal **111**, 1478 (2016).
- [46] G.-K. Xu, X.-Q. Feng, and H. Gao, Biophysical Journal **114**, 701 (2018).
- [47] R. Aris, *Vectors, Tensors, and the Basic Equations of Fluid Mechanics*, 1st ed. (Dover Publications, Inc., New York, 1989).

- [48] C. Canuto, M. Y. Hussaini, A. Quarteroni, and T. A. Zang, *Spectral Methods: Fundamentals in Single Domains*, 1st ed. (Springer, New York, 2006).
- [49] S. Bulent Biner, *Programming Phase-Field Modeling*, 1st ed. (Springer, Cham, 2017).